Vaporization Kinetics of Electrically Exploded Tungsten Wires at the Heating Rates of 1 - 10 K/ps[1]

A. D. Rakhel[2, 3], and G. S. Sarkisov[4]

Experimental results on electrically exploded tungsten wires at the heating rates of 1 to 10 K/ps and their interpretation in the framework of a one-dimensional magneto-hydrodynamic model are presented. The main features of both melting and volume vaporization observed in these experiments are discussed. It is shown that no superheating of solid tungsten takes place at these heating rates (within a 10 to 20 % experimental uncertainty). Comparison of different quantities measured and calculated by means the model evidences that the volume vaporization starts close to a binodal line. A relaxation time for the volume vaporization in the tungsten wires used is estimated to be substantially smaller than 1 ns.

KEY WORDS: superheating; melting; vaporization; exploding wires; tungsten.

1. INTRODUCTION

Kinetics of volume vaporization in electrically exploded wires has been discussing in the literature for a long time. Beginning from the work of Bennett [1] it is usually assumed that liquid phase is essentially superheated. Bennett developed a so called vaporization wave model to describe the liquid-vapor phase transition caused by an intense Joule heating. The model was based on the assumption that vaporization starts from the surface of a wire heated by an electrical current pulse and propagates to its axis as a wave. In the wave front the wire material undergoes a transition from the superheated liquid state to a two-phase liquid-gas state close to local thermodynamic equilibrium. The possibility of boiling in the bulk of the superheated liquid was considered to be less probable as far the boiling kinetics and inertia effects in the two-phase mixture prevent such scenario. The typical heating rates for experiments performed by Bennett are of the order of 10^9 K·s^{-1}, what corresponds to a characteristic time of about 1 μs.

Martynyuk has introduced a hypothesis about the phase explosion [2] to explain the exploding wire dynamics at these heating rates. It is assumed that a metal wire remains homogeneous during an initial stage of the heating process when the wire material is in a solid state region and then in the liquid states before boiling begins. The boiling starts when the liquid reaches the states close to a spinodal line. Such vaporization should behave like an explosion as far the internal energy of the superheated liquid approaches the sublimation energy.

On the other hand in the work [3] devoted to investigation of unloading of metals initially compressed by a shock wave the start of boiling was clearly detected and used to determine the boiling curve position at high temperatures. In these experiments porous specimens were subjected to the shock compression and the velocity of the rear specimen surface was measured when the shock wave emerged at it. Due to beginning of the volume vaporization the velocity showed an additional increase in comparison with that for a superheated liquid. In paper [3] a relaxation time for the volume vapori-

---

[1] Paper presented at the Fifteenth Symposium on Thermophysical Properties, June 22-27, 2003, Boulder, Colorado, USA.

[2] Institute for High Energy Densities, Izhorskaya 13/19, Moscow 125412, Russia

[3] To whom correspondence should be addressed. E-mail: **savlab@iht.mpei.ac.ru**

[4] Ktech Corporation, Albuquerque, NM 87106, USA

zation was estimated to be on the order of 1 ns or even less.

Thus, the dynamic experiments were interpreted by the authors [1], [2] and [3] using the essentially different points of view. It should be noted that no direct evidences of the remarkable superheating achieved in experiments [1, 2] are provided. The main goal of the present study is to find such evidences or to confirm the assumption [3] that the boiling starts close to the binodal line. The point is that the volume vaporization kinetics plays a very important role in the entire exploding wire dynamics [6]. For many applications a model should be developed describing the hydrodynamic flow caused by an exploding wire. This model should answer some specific questions, in particular about the distributions of physical quantities across the plasma column formed by the wire [4, 5]. To answer the questions the volume vaporization kinetics should be described correctly in such a model.

In the work [6] the maximal heating rate of 10^{11} K·s^{-1} was achieved. No superheating effects were detected in those experiments for tungsten wires manufactured without any purification procedure (to remove the nucleation centers). Using the relaxation time for the volume vaporization of 1 ns from [3], one can obtain a superheating of the order of 100 K for experiments [6] what is a very small value to be detected. It is of interest to answer the question: what is the heating rate ensuring the maximal superheating, i.e. achievement of the sates close to the spinodal line? It is easy to see that at this heating rate the temperature increases starting from the boiling point temperature $T_b(P)$ to the spinodal temperature $T_s(P)$ for 1 ns or less. In the case of tungsten this one obtains a heating rate of about $7.7 \cdot 10^{12}$ K·s^{-1}. In this estimate we used for the normal boiling point temperature of tungsten a value of 5,830 K [7], and for the spinodal temperature a value of $T_s \approx 13{,}500$ K. The spinodal temperature was calculated by van der Waals model and the value of T_s at zero pressure was used:

$$T_s(0) = \frac{27}{32} T_c \qquad (1)$$

where T_c is the critical temperature of tungsten ($T_c \approx 16{,}000$ K, [6]).

The so high heating rates estimated above were used in the recent exploding wire experiments [8]. In the paper we present theoretical and experimental results of investigations of the exploding wire dynamics at the heating rates of 10^{12} - 10^{13} K·s^{-1}. Experiments with tungsten wires in the air have been performed using the installation [8]. The heating dynamics is described in the framework of a self-consistent one-dimensional magneto-hydrodynamic (MHD) model [6, 9]. It is demonstrated that the model describes adequately (with an uncertainty of 10%) all the dependencies measured over the entire range of the heating rates. The main features of the volume vaporization kinetics have been established. It is shown that both the melting and the volume vaporization (boiling) start close to the corresponding equilibrium phase boundaries even at the maximal heating rates applied.

2. EXPERIMENTAL SETUP

A schematic diagram of the electrical circuit used is presented in Fig. 1. A 100 kV-Maxwell 40151-B pulse generator with a 7 nF capacitor bank and a 60 kV charging voltage provided an electrical current pulse. A 9 m long 50 Ω coaxial cable delivered the current pulse from the generator to a wire. The wire was placed in a coaxial target unit with four diagnostic windows. Figure 2 demonstrates the coaxial target unit and the positions of a current and voltage detector. The down-stream current through the wire

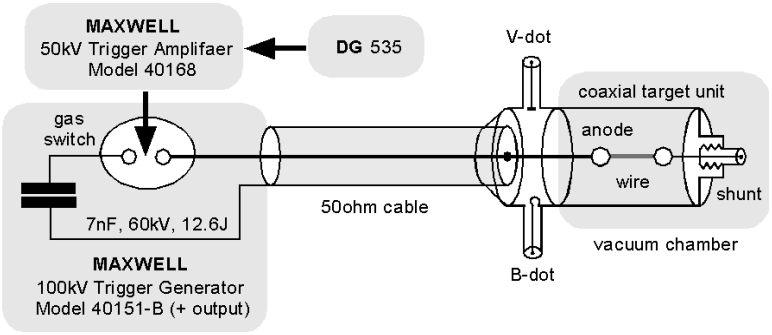

Fig. 1 Schematic diagram of electrical circuit.

was measured with a 2-GHz bandwidth 0.1-Ω coaxial-shunt resistor. The anode-ground voltage was measured with a V-dot (capacitive divider). A Si PIN-diode with a 1 ns rise time monitored the light emission power from the wire. All electrical waveforms were recorded with a 4-channel, 1-GHz digital scope, Tektronix TDS 684C.

An SBS-compressed Nd:YAG Q-switch laser with 120 mJ energy at 532 nm and with 150 ps pulse duration (EKSPLA SL-312) was used for simultaneous frame image shadowgraphy and interferometry of an entire column formed by the wire. Streak camera (Hamamatsu C1587-01) radius-time diagrams of the exploding wire were obtained using a high-power pulse diode laser back lighter (Power Technology, IL30C, 905nm, 10W, 200ns) and an appropriate relay optics.

An experimental voltage waveform consists of a resistive and inductive part. For a fast current rate (~150 A/ns) experiment it is of importance to know the inductive voltage to get a true value for the remained resistive part. For the ns-time scale experiments this is a rather complicated task. To get a right inductance of the coaxial target unit we have measured the voltage waveforms for a shorted

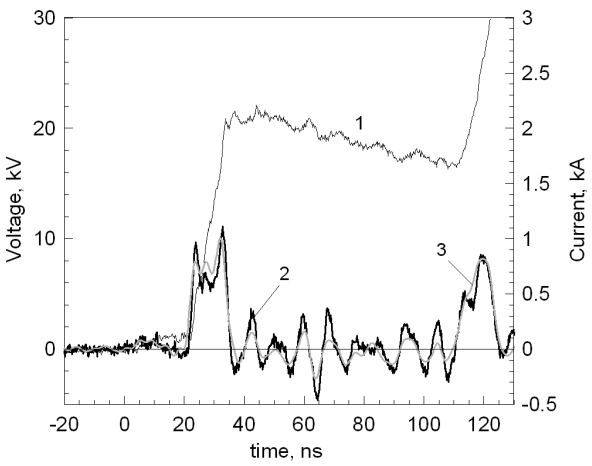

Fig. 3. Current (1) and voltage (2) waveforms measured for short circuit load. Inductive part of the voltage (3) calculated demonstrates a good agreement with the measured waveform.

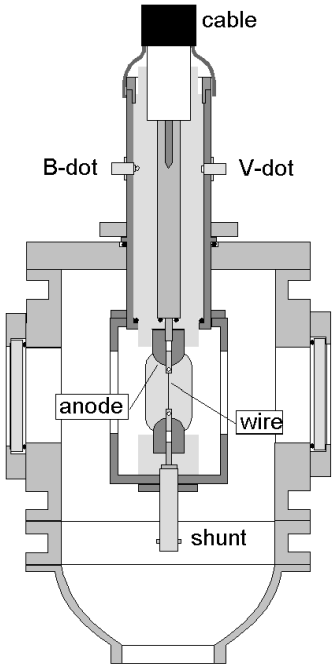

Fig. 2 Vacuum chamber with coaxial target unit.

circuit when a copper wire of a 2 mm diameter and 2 cm long was placed instead of the specimen. The sample shorted circuit waveforms of the voltage, current and a reconstructed inductive voltage $L_3\, dI/dt$ are presented in Fig. 3 (L_3 is the target unit inductance). The best fitting for the inductive voltage we got for $L_3 \approx 50$ nH. The

experimental curves presented in Fig. 3 demonstrate correctness of the measured current and voltage waveforms. In our experiments with tungsten wires discussed below the wire inductance was calculated by

$$L_w = 2l \ln(2l / d_0) \qquad (2)$$

where l is the wire length and d_0 is its initial diameter. The experiments were carried out with tungsten wires having a diameter of 16.2 μm and length of 2 cm. These wires were manufactured by California Fine Wire Company[5] with declared purity of 99.95%.

3. ELECTRICAL CIRCUIT ANALYSIS

As far the measurements of the current trough the wire should be performed with a high precision it was of importance to find out a real uncertainty of the measurements. To solve the task, the shorted circuit current waveforms were calculated and compared with the measured ones.

Let us now discuss the approach used in these calculations. The pulser and the target unit was treated as quasistationary circuits as far their geometrical dimensions are relatively small (of the order of 10 cm) while for the cable the telegraphic equations were solved. The current in the pulser circuit $I(t)$ satisfies the following equation:

$$\frac{d^2 I}{dt^2} + \gamma_1 \frac{dI}{dt} + \omega_1^{\,2} I = 0 \qquad (3)$$

with $\gamma_1 = Z_2 / L_1$, and $\omega_1 = 1/\sqrt{L_1 C_1}$ where L_1 is the pulser circuit inductance, C_1 is the capacitance of the capacitor bank, and Z_2 is the cable impedance. Here and below we designate index *1* to the pulser circuit parameters, *2* to that of the cable, and *3* to the target unit. The solution of Eq. (3) has a form

$$I_1(t) \approx \frac{U_0}{Z_2}\left[\exp\left(-\frac{t}{C_1 Z_2}\right) - \exp(-\gamma_1 t)\right] \qquad (4)$$

where U_0 is the charging voltage of the capacitor bank. In the case, the cable attenuation is small the current wave in the cable propagates without transformations. For any wave generated in this case the following relation is valid: $V = \pm \upsilon I$, where υ is the wave velocity ($\upsilon = 1/\sqrt{L_2 C_2}$), and the sign plus corresponds to the wave moving from the pulser to the target unit. The total current through the target unit is a superposition of the incident current wave $I_i(t)$ and a reflected one $I_r(t)$, $I = I_i - I_r$. It can be shown that the total current trough the target unit satisfies the following equation:

$$\frac{d^2 I}{dt^2} + \gamma_3 \frac{dI}{dt} = 2\gamma_3 I_i(t) \qquad (5)$$

where $\gamma_3 = Z_2 / L_3$. In Eq. 5 the dependence $I_i(t)$ is a given function of time, namely the function (4) should be taken. The solution of Eq. (5) satisfying the initial condition $I(0) = 0$ is

$$I(t) = \frac{\dfrac{U_0}{Z_2}}{\gamma_3 - \dfrac{1}{C_1 Z_2}}\left[\exp\left(-\frac{t}{C_1 Z_2}\right) - \exp(-\gamma_3 t)\right] -$$

[5] http://www.calfinewire.com

$$-\frac{\frac{U_0}{Z_2}}{\gamma_3-\gamma_1}\left[\exp(-\gamma_1 t)-\exp(-\gamma_3 t)\right] \qquad (6)$$

In Fig. 4 this temporal dependence is compared with the measured one (inductance L_1 was taken to be 250 nH). The analytic solution is valid only by the instance of time when the current wave reflected from the target unit and then from the pulser returns back. The interval of time between the neighbor current maxima is equal just to the ration of the double cable length to the wave velocity, i.e. $2l_2/\upsilon \approx 90$ ns (for RG 220 cable used $\upsilon \approx 20$ cm·ns^{-1}). To describe the current evolution in the μs-time scale a complete model of the electrical circuit was developed. In the model the pulser and the coaxial target unit were represented by several *RCL* circuits. For the cable the telegraphic equations were solved taking into account its real attenuation. The dashed line in Fig. 4 corresponds to the model calculations. As one can see the main features of the current pulse are described by the model well. Basing on the comparison we conclude that the electrical circuit has well defined parameters and the current measurements were performed with a fairly good precision (better than 2-3 % as to the current magnitude). This is the reason why all the MHD computations presented below were performed for prescribed temporal dependences of the current through the wire.

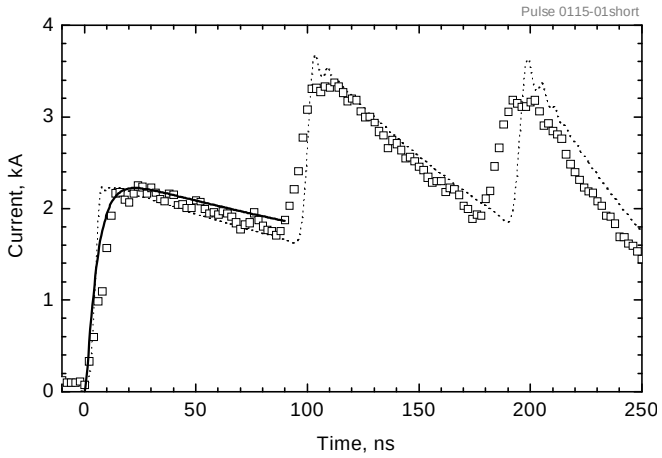

Fig. 4. Comparison of temporal dependences measured (squares) and calculated (lines) for the electrical current in shorted circuit: solid line, analytic solution by Eq. (6); dashed line, numerical solution of the complete set of equations for the electrical circuit.

4. MAGNETO-HYDRODYNAMIC MODEL

To describe the hydrodynamic flow generated by a current pulse applied to a wire the one-dimensional magneto-hydrodynamic model [6, 9] was used. The corresponding set of equations of the model consists of the local laws of conservation of mass, linear momentum and energy together with Maxwell's equations. It is supposed that Z-pinch symmetry is kept during the heating process. For the coordinate system the z-axis of which is directed along the axis of a rectilinear wire, all physical quantities are functions of the radius-vector *r* and the time *t* only. The only nonzero component of the velocity for this flow is the radial component. The electrical current density has only a component along the z-axis, and the magnetic field strength has only an azimuthal component.

It is easy to see that effects of the heat conduction, viscosity and radiation may be neglected under these conditions, and therefore the corresponding terms were dropped in the equations of the model. The evaporation from the wire surface can be also neglected in this case, as far this process is governed by the heat conduction from

the bulk to the surface which loses the high energy molecules. Indeed, the characteristic spatial scale for the heat conduction is on the order of $\sqrt{\chi t}$ where χ is the thermal diffusivity of liquid tungsten and t is the characteristic time scale for the heating process. For $t \sim 1$ ns and $\chi \sim 0.1$ cm^2·s^{-1}, we obtain for the thickness of the layer where the temperature is nonuniform due to the surface vaporization a value of the order of 0.1 μm. This is much smaller than the radius of the expanded wire in a liquid state, what is 12 – 16 μm.

The hydrodynamic flow was computed for two regions: the wire and surrounding air. We assumed that the substances do not mix with each other at the boundary. Other details concerning the model, the numerical methods used can be found in [6, 9].

Thermodynamic functions of tungsten in the region of the liquid-vapor phase transition were obtained using an equation of state model from Ref. 10 with some modifications to reproduce the behavior of thermodynamic functions of tungsten at high temperatures [6]. Magneto-hydrodynamic computations performed in [6] have allowed to us establishing such experimental conditions under which an expanding wire remains homogeneous down to a density four times lower than the standard solid density of tungsten. These heating regimes were used to investigate thermophysical properties of tungsten at substantially higher temperatures and pressures than those attained in slower experiments [11, 12, 13]. The thermal expansion coefficient of liquid tungsten along with its critical point parameters were obtained in that work. The fitting parameters of the EOS model were chosen in [6] using these experimental data. No additional corrections in the EOS model were made in the present work.

The information on the electrical conductivity of tungsten in the liquid-vapor phase transition domain is also required for our computations. The basic idea of the approach to construct a conductivity dependence on the density and temperature in this domain is the following. In the condensed state (the solid state and liquid at the low temperatures, $T<T_c$) the dependence was taken from experiments using an approximation of the experimental data obtained in [11, 12, 13] and [6, 9] as well. In the gaseous state at high temperatures (ideal gas) the conductivity was calculated using a well developed theoretical method. In the inter-medium region an interpolation was used. In the present work we will focused on the liquid-vapor phase transition at the pressures which are smaller than the critical pressure P_c (11 ± 2 kbar [6]). Therefore, in this case one may expect that the dependence of the electrical conductivity in the gaseous state is not of importance. It is assumed that in the two-phase liquid-gas region of the phase diagram the phases constitute a fine dispersed mixture. The conductivity of the mixture was calculated by means of the effective medium formulae [14].

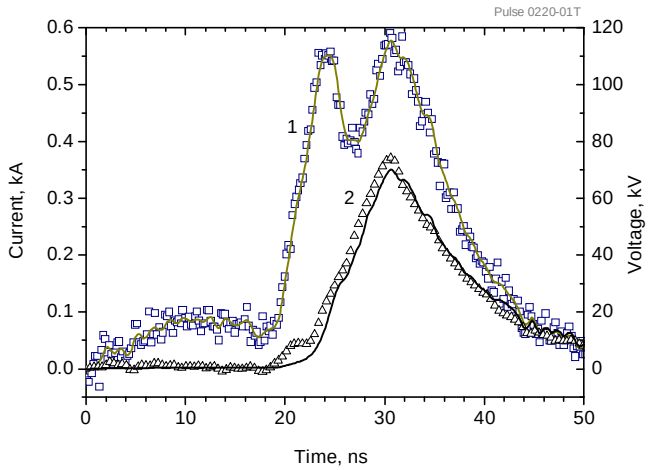

Fig. 5. Current through the wire (1) and resistive voltage drop across it (2): marks, experiment; voltage solid line, modeling result; current solid line, approximation of the experimental data used in this modeling.

5. MELTING

Temporal dependencies of the current through the wire

and the resistive part of the voltage drop across its length are presented In Fig. 5. As one can see, the discrepancies between the calculated and measured voltage don't exceed about 10% in the time interval beginning from 25 to 40 ns. The solid line for the current dependence in Fig. 5 was obtained by means of an approximation of the experimental data and was used in the MHD computations as a given function. Complementary laser shadowgrams of the wire at different moments of time are presented in Fig. 6(a, b, c). As one can see, the column formed by the wire expands uniformly during a sufficiently

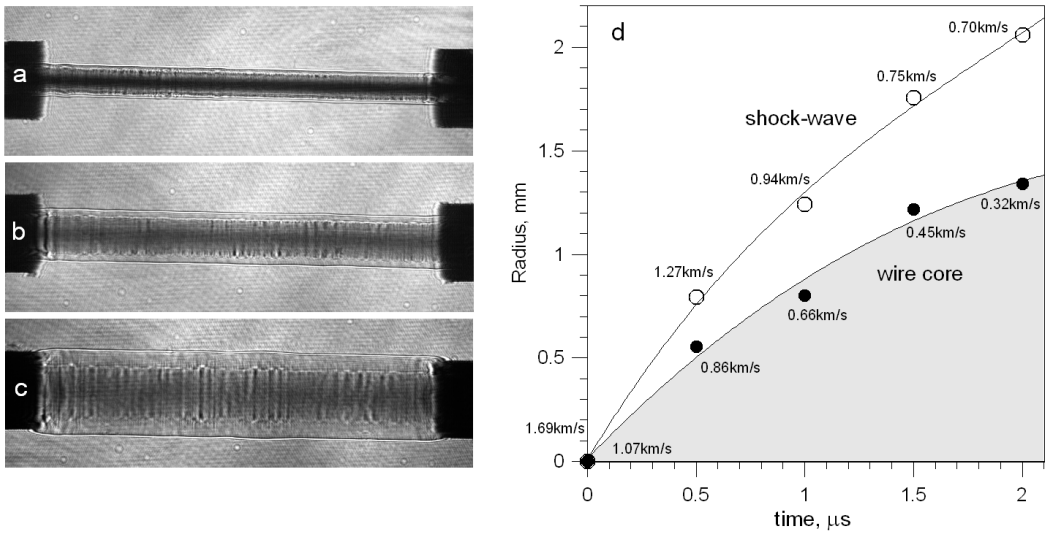

Fig. 6. Laser shadowgrams of an exploding W wire of 16.2 mm diameter and 2 cm long at different moments of time: (a) at 500 ns, (b) 1000 ns, (c) 2000 ns from the voltage peak. Temporal evolution of the shock-wave and wire core diameters for different experiments (d).

long period of time. Nevertheless, in the shadowgrams it can be seen an expanding wire core with an unstable boundary following a shock wave. The shock wave has a stable boundary and size along the wire length. Figure 6(d) demonstrates the size of the shock wave and the wire core for different moments of time taken from several similar experiments. The shock wave moves 1.5 - 2 times faster than the wire core. The expansion of both the shock wave and the core occurs with a deceleration. The shock wave starts at a velocity of 1.7 km·s^{-1} (1.07 km·s^{-1} for the core) and then decreases to about 0.7 km·s^{-1} at the moment of 2 μs (0.32 km·s^{-1} for the core respectively).

In the main the paper deals with the vaporization kinetics. Nevertheless, melting dynamics and thermophysical data of liquid tungsten measured in our experiments were also carefully analyzed. On the one hand the reason was to cast a light on the melting kinetics at the high heating rates achieved in these experiments. On the other hand, the measured data were compared with reliable literature data to estimate the corresponding uncertainties of our measurements. The question about the melting kinetics can be formulated as follows: is it possible to indicate the effects of superheating of the solid phase. Our approach was based on the well-known fact that the dependence of a tungsten wire resistance on enthalpy shows remarkable breaks at the beginning and end of melting [11, 12, 13]. Therefore the current and voltage signals should show some peculiarities in their temporal dependencies at the corresponding times. Our voltage measurements were not sensitive enough to observe these features and therefore they were looked for in the current versus enthalpy dependencies.

In Fig. 7 the current trough the wire and the resistive voltage drop are shown as functions of enthalpy. It is obvious, that there are two clear expressed breaks in the

current dependence at the values of enthalpy reasonably correlating with the solid (0.64 $kJ \cdot g^{-1}$) and liquid phase enthalpy (0.92 $kJ \cdot g^{-1}$) at the melting point measured in [15]; the scatter of the data presented in [11, 12, 13, 15] in respect to these enthalpies is 6%. Therefore, we can emphasize that there are no shifts in the solid and liquid phase enthalpy at the melting point in comparison to the data obtained at the heating rates which are three orders of magnitude less. This testifies that no superheating (within a 10 to 20% uncertainty) of solid tungsten is observed in our experiments[2].

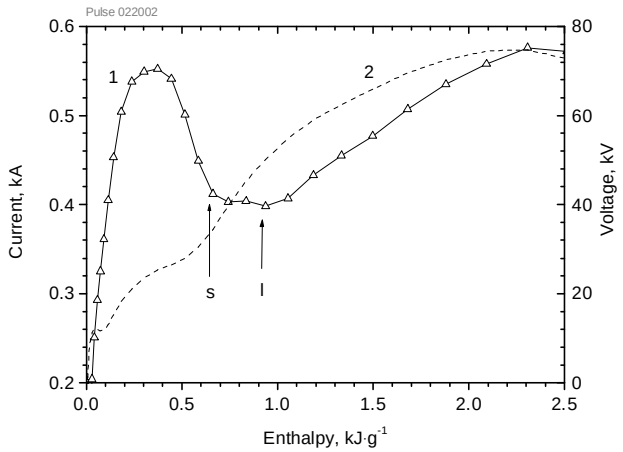

Fig. 7. Current through the wire (1) and resistive voltage drop across it (2) versus specific enthalpy. The arrows indicate the literature data for the solid (s) and liquid (l) state enthalpy at the melting point.

In general, the effects of superheating depend on the crystal structure of the specimen and, in particular, on the crystallite dimensions. What should be the average size of the crystallites that the superheating is within the 10% level in respect to the solid phase enthalpy at the melting point? To answer the question we should make some estimates. The melting fronts starting at the crystallites boundaries are governed by the heat conduction transport. In the case the melting takes a sufficiently long time the superheating is small. Therefore if the average crystallite size is smaller than $4\sqrt{\chi t_m}$ (t_m is the melting duration) the superheating is small. For the experiment presented in Fig. 7, $t_m \approx 2$ ns and, therefore the crystallites are much smaller than about of 1 μm. This is a reasonable value as far the initial wire diameter is given by the manufacturer with a precision of 0.1 μm.

6. VAPORIZATION

The discussion of the vaporization kinetics we start from Fig. 8 in which the pressure and the so-called resistivity without volume correction are shown as functions of specific enthalpy. This resistivity is a directly measured quantity and, on the other hand, it can be compared with the literature data. This quantity (R^*) is proportional to the ratio of the density ρ to electrical conductivity σ (in the case the specimen remains homogeneous and its length is constant):

$$R^* = \frac{1}{\sigma}\frac{\rho}{\rho_0} \qquad (7)$$

(ρ_0 is the standard solid density).

As one can see in Fig. 8(a), the pressure in the specimen (curve 1) varies not monotonously: there are two maxima. This is a result of the temporal dependence of the Joule heating power having also two maxima due to the specific current temporal dependence shown in Fig. 5. To explain the main features of the pressure behavior an

[2] More accurate estimate of the superheating can be performed calculating the heat of fusion, i.e. difference between the enthalpies at the breaks. In this case the errors in determining the absolute values of the enthalpies will be compensated.

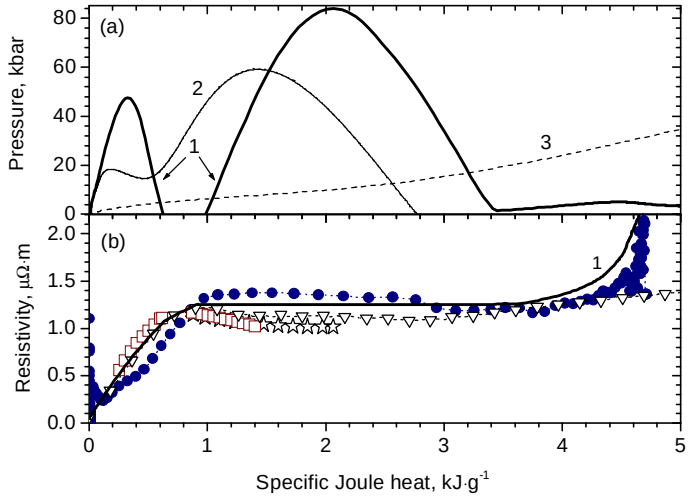

Fig. 8. Pressure (a) and resistivity without volume correction (b) versus specific Joule heat released. Thick lines (1), modeling result for this work experiment; thin line (2), pressure calculated by analytic formula (9); dashed line (3), modeling result for experiment [9]. Closed circles, this work experiment; open triangles, [9]; open squares, [12]; stars, [11].

analytic solution of the hydrodynamic equations obtained in [16] is used. The solution was deduced for the case $c_s t \gg a(t)$ where c_s is the speed of sound, $a(t)$ is the specimen radius and t is a characteristic time scale. In this case the density profile in the specimen can be presented as a sum of a homogeneous term $\rho_h(t)$ depending only on time and a small inhomogeneous term $\rho'(r,t)$:

$$\rho(r,t) = \rho_h(t) + \rho'(r,t) \quad (8)$$

The approach is valid when the substance is in a condensed state so that the pressure effect is relatively small (see Ref. 16 for explanations). For a wire subjected to the pulse heating the pressure can be presented by

$$p(r,t) \approx \frac{\rho_0 a_0^{\,2}}{2a}\frac{d^2a}{dt^2}\left[1-\left(\frac{r}{a}\right)^2\right] \quad (9)$$

where a_0 is the initial radius of the wire. The thin line in Fig. 8(a) corresponds to the pressure at the wire axis ($r = 0$) calculated by means of formula (9). In this calculation we used the temporal dependence of the Joule heating power as an input function. The following dependence of the liquid tungsten density versus specific enthalpy was used:

$$\rho = \rho_0(1-\alpha w) \quad (10)$$

where w is the specific enthalpy measured from standard state, and α is a constant which can be expressed through the thermal expansion coefficient and the heat capacity c_P ($\alpha \approx 0.12$ g·kJ^{-1} [6]). Dependence (10) was proved in [6] to be valid in a wide density range. The Joule heat released in the specimen as a function of time was determined from the measured current and voltage and was used then to get the derivative d^2a/dt^2, as far the product $\rho_h(t)a(t)^2$ is a constant in this approximation. The difference between the Joule heat and the enthalpy is small under these conditions and therefore it can be neglected. As a result, the following expression can be obtained for the derivative (the radius acceleration):

$$\frac{1}{a}\frac{d^2a}{dt^2} = \frac{1}{2}\left[\frac{\alpha}{1-\alpha w}\frac{d^2w}{dt^2} + \frac{3}{2}\left(\frac{\alpha}{1-\alpha w}\frac{dw}{dt}\right)^2\right] \quad (11)$$

As one can see the pressure calculated by (9) agreed well with that obtained by means of the complete hydrodynamic model. Nevertheless, the absolute values of the pressure given by the analytic solution are substantially lower. This is due to the delay effects being of importance under these conditions. Indeed, the acoustic time a/c_s is about of 2 ns for the solid wire at room temperature and increases to about 6 ns for the melted wire at the normal boiling point temperature; the value of the liquid tungsten

sound speed at the normal boiling point of 2.5 km·s^{-1} was taken from [13]. As it follows from Fig. 5, the half width of the current peaks is comparable with the acoustic time estimated. Therefore, the approach developed in [16] is, strictly speaking, not correct in this case. The inertia effects are underestimated by formula (9).

To show the contribution of the pinch-effect the magnetic pressure p_H was calculated

$$p_H(r,t) \approx 10^{-3} Ij\left[1-\left(\frac{r}{a}\right)^2\right] \qquad (12)$$

where I is the current magnitude and j is the current density (SI units are used). Formula (10) was obtained for the quasistatic limit, i.e. when $c_s t \gg a$. In fact, the thin line presented in Fig. 8 (a) is a superposition of two lines: the pressure obtained by (9) and the total pressure, i.e. the sum of the inertia pressure giving by (9) and the magnetic pressure (12). It seems to be clear, that the magnetic pressure can be neglected under these conditions.

The next important thing which can be inferred from Fig. 8 is the good agreement between our measurements and those performed in [9]. The corresponding pressure curves calculated for these experiments cross at an enthalpy of 3.1 kJ·g^{-1}. Just at this point the corresponding resistivity curves nearly coincide to within the experimental uncertainty. The further pressure evolution for this work experiment shows continuing decrease followed by a plateau at 3.3 kbar. This plateau is formed when the substance enters the two-phase liquid-gas region and the boiling starts.

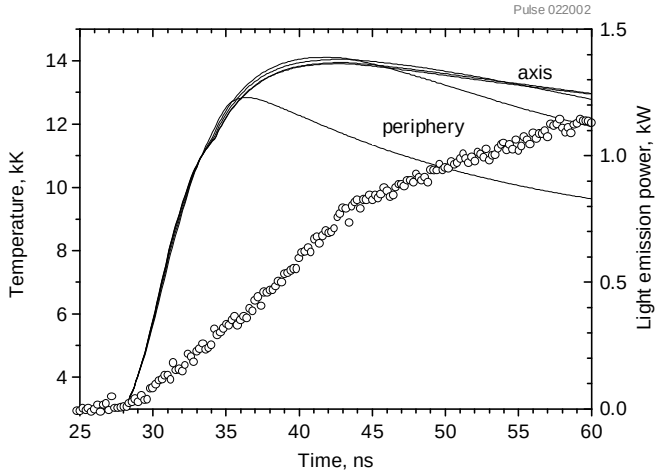

Fig. 9. Temperature for several radial layers (lines) and the light emission signal (circles) as functions of time.

The point is that the calculations were performed for the case the boiling starts close to the binodal line. The resistivity measured in our experiment shows a rise very similar to that predicted by the model. It should be noted that the pressure line shown in Fig. 8(a) corresponds to the specimen axis, the boiling in the periphery regions starts earlier. The main conclusion which can be drawn from Fig. 8 is the following: the one-dimensional MHD model assuming that vaporization starts close to the binodal line is in a good agreement with the experimental data.

To prove that the vaporization kinetics effects are described by the model correct in Fig. 9 the temperature calculated for several radial layers in the specimen together with the light emission waveform are depicted. The layers represent only five cells of the spatial mesh among 100 – 300 cells in the wire region used in our computations. Each layer contains a fixed mass of the substance, i.e. corresponds to a specific Lagrangian coordinate. The clearly expressed break in the light emission signal correlates well with the maximum in the near-axis region temperature achieved at an instance of 42 to 43 ns. As far the specimen diameter grows the area from which the light is captured by

the diode increases this is why the light emission signal grows even after the temperature approaches a nearly constant value. It appears that the peripheral layers in which the temperature decreases remarkably becomes transparent and the light emission from the inner regions is captured. The similar behavior for tungsten wires when a peripheral layer starts to boil and then becomes transparent was discussed in [6]. This behavior was used there to estimate the liquid core temperature where the pressure was high enough to prevent boiling.

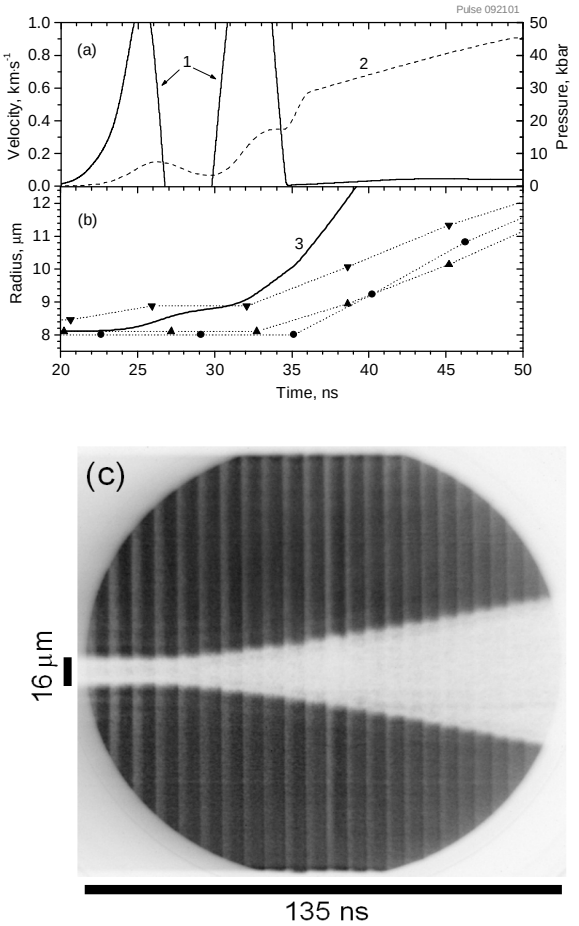

Fig. 10. Velocity at the wire surface and pressure at its axis calculated (a), radius measured and calculated (b) and streak image of an exploding wire (c) as functions of time. Thick line (1), pressure; dashed line (2), velocity; marks connected with lines, streak image data for three similar experiments; thick line (3), calculated radius.

A series of experiments was performed to measure the wire diameter evolution during the heating process. The streak image shadowgraphy was used. In Fig. 10 the measured and calculated wire radius as functions of time are presented together with the calculated pressure at the wire axis and the velocity at its surface. It is obvious that the expansion observed in the experiment starts just after the pressure drop in Fig. 10(a). The velocity jump due to the start of boiling shown in Fig. 10(a) and other peculiarities couldn't be recognized in the radius measurements because of a poor temporal resolution of the streak shadowgraphy used. The simulation predicts a higher expansion velocity (~ 0.6 km·s^{-1}) compared with the measured one (~0.4 km·s^{-1}). It happens because in this series experiments a shunting discharge between the anode and ground was developed. The energy deposition into the wire was terminated just after the voltage maximum. Despite of this anode-ground breakdown the streak image data demonstrate a reasonable correlation with the MHD simulation results. In other experiments when breakdown problems were absent (figs. 5,7 and 9) the initial expansion velocity was pretty close to calculated value (see Fig. 6(b)).

7. CONCLUSIONS

It has been demonstrated that the exploding wire technique utilized in this work allows performing representative measurements at the heating rates of 10^{12} to 10^{13} K·s^{-1}. It seems to be clear that the tungsten wires subjected to these heating rates can be rather

accurately described in the frame work of a one-dimensional MHD model. It is shown that such measurements together with a proper theoretical description of the dynamics can cast a light on some longstanding physical problems. In particular this belongs to the melting and volume vaporization kinetics in refractory metals.

No shifts of the solid and liquid phase enthalpy at the melting point were detected for tungsten at the heating rates of 10^{12} to 10^{13} $K \cdot s^{-1}$. This evidences that no superheating effect (within a 10 to 20 % experimental uncertainty) takes place under these conditions. Comparison of different quantities measured and calculated by means the one-dimensional MHD model has shown that the volume vaporization starts close to the binodal line. The relaxation time for the volume vaporization in the tungsten wires used is estimated to be much smaller than 1 ns.

REFERENCES

1. F.D. Bennett, in *Physics of High Energy Density*. P. Caldirola and H. Knoepfel, eds. (Academic Press, New York and London, 1971), Part. 7.
2. M. M. Martynyuk, *Int. J. Thermophys.* **14**(3): 457 (1993).
3. L. V. Altshuler, A. A. Bakanova, A. V. Bushman, I. P. Dudalapov, V. N. Zubarev, *Zh. Eksp. Teor. Fiz.* **73:** 1866 (1977).
4. K. M. Chandler, D. A. Hammer, D. B. Sinars, S. A. Pikuz, T. A. Shelkovenko, *IEEE Trans. Plasma Sci.* **30**(2):577 (2002).
5. A. W. DeSilva and J. D. Katsouros, *Int. J. Thermophys.* **20**(4): 1267 (1999).
6. A. D. Rakhel, A. Kloss, and H. Hess, *Int. J. Thermophys.* **23**(5): 1369 (2002).
7. D. R. Lide and H. P. R. Frederikse eds, *CRC Handbook of Chemistry and Physics*, (CRC Press, Boca Raton, Ann Arbor, London, Tokyo, 1993-1994).
8. G. S. Sarkisov, P. V. Sasorov, K. W. Struve, et al., *Phys. Rev. E* **66**: ??? (2002)
9. V. N. Korobenko, A.D. Rakhel, A. I. Savvatimskiy, and V. E. Fortov, *Plasma Physics Reports* **28**(12): 1008 (2002).
10. D. A. Young, Lawrence Livermore Laboratory Report No. UCRL-52352 (1977).
11. U. Seydel, W. Fucke, and H. Wadle, Die Bestimmung thermophysikalischer Daten flüssiger hochschmelzender Metalle mit schnellen Pulsaufheizexperimenten (Verlag Dr. Peter Mannhold, Düsseldorf, 1980).
12. A. Berthault, L. Arles, and J. Matricon, *Int. J. Thermophys.* **7**:167 (1986).
13. R. S. Hixson and M. A. Winkler, *Int. J. Thermophys.* **11**:709 (1990).
14. R. Landauer, *J. Appl. Phys.* 23: 779 (1952).
15. E. Arpaci and M. G. Frohberg, *Z. Metallkd.* **75**:614 (1984).

A. D. Rakhel, *Int. J. Thermophys.* **17**(5):1011 (1996).